Solid-state amorphization in Al-Pt multilayers by low-temperature annealing

B. Blanpain and L. H. Allen

Department of Materials Science and Engineering, Bard Hall,
Cornell University, Ithaca, New York 14853-1501

J.-M. Legresy

Centre de Recherches de Voreppe, Société Anonyme, Boîte Postale 27, 38340 Voreppe, France

J. W. Mayer

Department of Materials Science and Engineering, Bard Hall,
Cornell University, Ithaca, New York 14853-1501

We report the solid-state amorphization reaction between crystalline Al and Pt layers. Multilayer samples were made by sequential evaporation of layers of Al and Pt. In the as-deposited state the sample contains an amorphous phase at the Al-Pt interfaces. This amorphous phase grows during vacuum annealing at temperatures between 150 and 220 °C. A first estimation of the composition range of the amorphous phase is given, and the thermodynamic, kinetic, and structural-stability criteria proposed for solid-state amorphization are discussed in relation to the Al-Pt system.

I. INTRODUCTION

Since Yeh et al.[1] observed vitrification by reaction of Zr$_3$Rh with hydrogen, solid-state amorphization (SSA) has been extensively investigated. Schwarz and Johnson[2] first reported the amorphization by interdiffusion between crystalline metallic layers in the La-Au system, and Herd et al.[3] showed that an amorphous silicide is formed in the reaction between Rh and amorphous Si. In his review Johnson[4] lists the binary systems where solid-state amorphization has been found to occur. These binary systems can be divided into two groups: metal-metal systems and metal-silicon systems. In the metal-metal systems, the main subgroup consists of SSA reactions of an early transition metal (Ti,Y,Zr,La,Er) with a late transition metal (Fe,Co,Ni,Cu,Au). The Co-Sn (Ref. 5) system, which also forms an amorphous alloy by interdiffusion, is the only metal system that does not fall in this subgroup. The criteria[4] proposed for solid-state amorphization are a large and negative heat of mixing, anomalous diffusion, and low mobility for one of the elements in the amorphous phase. In addition, the Egami criterion[6] states that the presence of an amorphous phase is only feasible if the atomic-size difference of the elements is substantial.

In this paper we show the solid-state amorphization between crystalline layers of two fcc metals Al and Pt, which do not meet all the mentioned criteria: their atomic radii are comparable and anomalous diffusion is absent.

Up to now little work has been done on Al-Pt amorphous alloys. Hung et al.[7] have reported the formation of an amorphous phase after room-temperature ion-beam mixing of Al-Pt thin films. In previous work,[8] we observed a dissolution reaction of Al into a coevaporated amorphous Al-Pt layer. We also noted the presence of an amorphous layer between a bilayer of Al and Pt in the as-deposited state. Here we show that the amorphous layer grows during low-temperature annealing (150–220 °C), consuming the crystalline Al and Pt layers.

II. EXPERIMENT

The Al-Pt multilayers were deposited by electron-beam evaporation in a cryogenically pumped system. For a typical evaporation, the base pressure was 1×10^{-7} Torr and remained in the 10^{-7}-Torr range during evaporation. Layers of Al and Pt were sequentially evaporated with deposition of 1.0 nm/s for Al and 0.15 nm/s for Pt. The sample configuration consists of five layers: three aluminum layers separated by two platinum layers. The thickness for the outside Al layers was between 15 and 25 nm and for the inside Al layer between 20 and 35 nm. The Pt-layer thickness was kept around 10 nm. We used both cleaved sodium chloride crystals and thermally oxidized Si wafers as substrates.

Rutherford-backscattering spectroscopy (RBS) was used to determine composition and film thickness. The films on the sodium chloride substrates were floated off in deionized water onto Cu grids for *in situ* transmission-electron-microscopy (TEM) annealing and TEM observation. The films on the oxidized Si wafers were used in *in situ* resistivity measurements, Auger-electron spectroscopy (AES) profiling, and x-ray diffractometry (XRD).

In this section we will discuss the results of experiments on three samples with different overall composition (see Table I). The composition of the samples was analyzed by RBS. Since the Al peak is superimposed on the signal of the sodium chloride substrate, a subtraction of the chlorine peak is necessary to integrate the counts of the Al peak. After the background subtraction, the Al/Pt ratio was then determined using the RUMP[9] program. The statistical error in the concentration determination (± 4 at. %) is mainly due to the background subtraction. In addition, we expect RBS to systematically underestimate the effective Pt atomic fraction, because

TABLE I. Summary of the relevant information of the Al-Pt multilayer samples A, B, and C. The amorphization products were obtained after *in situ* TEM annealing for 15 min at 200 °C. The approximate crystallization temperature was determined at the first sign of nucleation during annealing in the TEM. After heating to 400 °C, the crystallization phase was identified by electron diffraction.

Sample	RBS composition (at. % Pt)	Amorphization reaction products	Crystallization temperature (°C)	Dominant crystallization phase
A	24 ± 4	$\alpha + Al$	≈360	Pt_8Al_{21}
B	25 ± 4	$\alpha + (Al)$[a]	≈270	$PtAl_2$
C	36 ± 4	$\alpha + Pt$	≈230	Pt_2Al_3

[a]The parentheses mean that some crystallites of Al remain (a small fraction, $\lesssim1\%$, of sample from diffraction pattern).

RBS includes the Al atoms in the surface oxide which are not available for the amorphization reaction. The effective concentration can, however, also be estimated from the equilibrium crystallization compounds, since the Al-Pt compounds are closely interspaced for the region of interest. A summary of the composition data is given in Table I.

With the AES profiling technique, we can also estimate the oxygen impurity level in the film. In the initial stage of the depth profile the presence of oxygen arises from a surface aluminum-oxide layer. Once the Ar ions have sputtered through the oxide, the oxygen level drops rapidly. In the bulk of the sample oxygen was still detectable with a level around 1 at. %.

III. RESULTS

The TEM specimens were then annealed *in situ* in a JEOL 200 CX microscope using the JEOL EM-SHH heating stage. Micrographs were taken in three different stages of the thermal history of the samples: in the as-deposited state, in the amorphized state, and in the crystallized state. We only present the micrographs for sample B (Table I), which illustrates these different steps.

The bright-field image of the as-deposited state presented in Fig. 1(b) shows the superposition of Al and Pt crystals. The Al grains range from 20 to 50 nm and are larger than the Pt grains (5–10 nm). The corresponding diffraction pattern and the microdensitometer trace [Fig. 1(a)] indicate the typical diffraction rings for the fcc structures. The Al rings are inside the corresponding Pt rings and are also spotty in appearance, as a result of the bigger Al crystals. In addition, broad rings originating from the amorphous phase are already discernible. This confirms the observation that already in the as-deposited state the amorphous phase has formed at the interface between the Al and Pt layers.[8]

The amorphized state was reached by heating the sample *in situ* in the TEM ($dT/dt \simeq 5$ °C/s) and holding them for 15 min at 200 °C. Amorphization starts noticeably around 150 °C. At 200 °C the reaction is faster, so we can assume that the amorphization reaction is completed after a 15-min period at this temperature. Sample B has been almost completely amorphized, as is clear by the selected-area-diffraction (SAD) pattern and the microdensitometer trace [Fig. 2(a)] together with the bright-field picture [Fig. 2(b)].

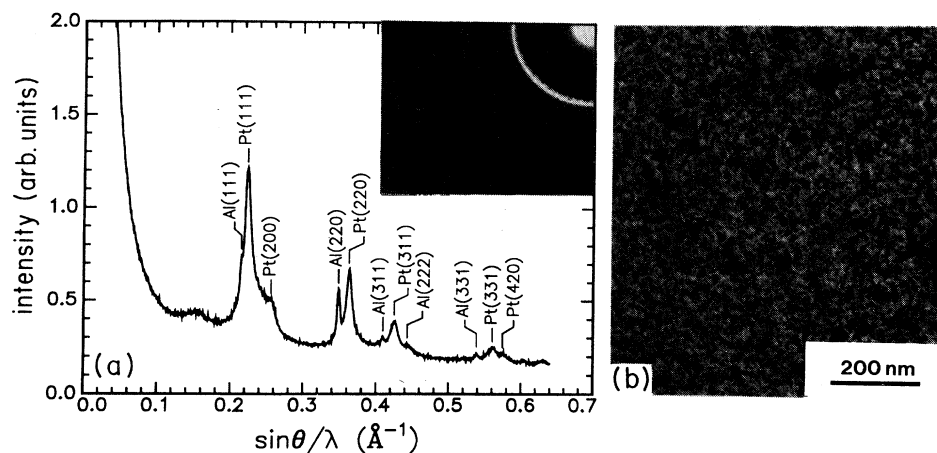The bright-field image mainly consists of low-contrast

FIG. 1. (a) Selected-area-diffraction pattern and microdensitometer trace of sample B in the as-deposited state. The sharp diffraction peaks can be identified as fcc Al and Pt peaks. Already we can observe the presence of broad diffraction rings of the amorphous phase (selected-area aperture diameter 3.5 μm). (b) Bright-field image of sample B in the as-deposited state. The diffraction contrast shows grains of Al (~20 nm) and Pt grains (~5 nm).
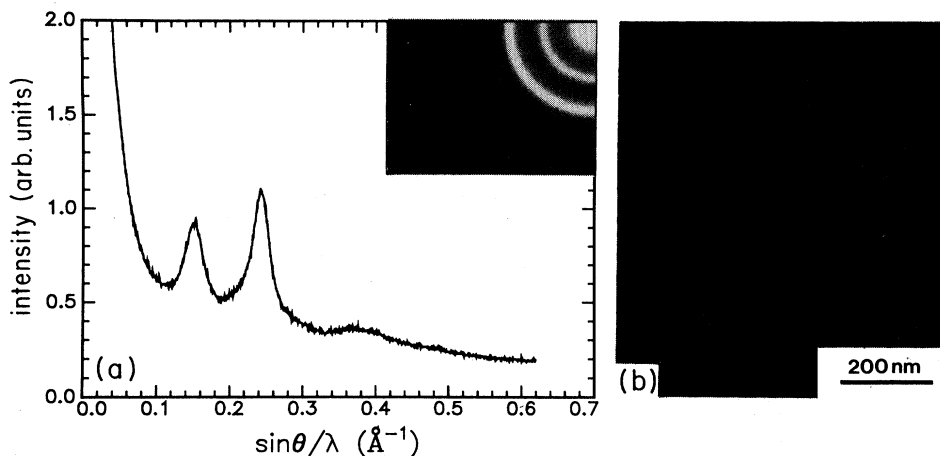
FIG. 2. (a) Selected-area-diffraction pattern of sample B in the amorphized state. Only broad rings of the amorphous alloy can be identified (selected-area aperture diameter 3.5 μm). (b) Bright-field image of sample B in the amorphized state. The contrast is mainly flat, as is typical for an amorphous phase, although some remnants of crystallites can still be distinguished.

regions due to the amorphous phase. However, some crystallites remain, but their presence is minute and there is no evidence of a sharp crystalline ring in the diffraction pattern. Remnants of crystals were also observed in the amorphized state in the case of Ni-Hf.[10]

The sample was then further heated above 400 °C. Around 270 °C the sample started crystallizing. After the crystallization the main crystalline structure is the cubic $PtAl_2$ phase [Figs. 3(a) and 3(b)]. In the microdensitometer trace all the lines are correlated with this structure. In the diffraction patterns some additional spots could be noticed, most likely due to the presence of a small amount of Pt_8Al_{21}.

For samples A and C, we will only give a description of the three different stages in the thermal annealing pro-

cess. The as-deposited state is very similar to that of sample B. However, in the amorphized state, samples A and B still show clear patches of crystalline regions. In sample A the crystals give rise to a clear fcc Al(111) textured diffraction ring in addition to the diffuse rings of the amorphous phase. In sample C the remaining crystals are fcc, Pt, as evidenced by the corresponding diffraction pattern. We conclude that sample A is on the Al-rich side and sample C on the Pt-rich side of the amorphous-phase region. Only sample B is in the composition range of the amorphous phase. The approximate crystallization temperatures of the different samples are listed in Table I. The trend is toward lower crystallization temperature for increasing Pt content. The dominant crystallization phase is Pt_8Al_{21} for sample A and
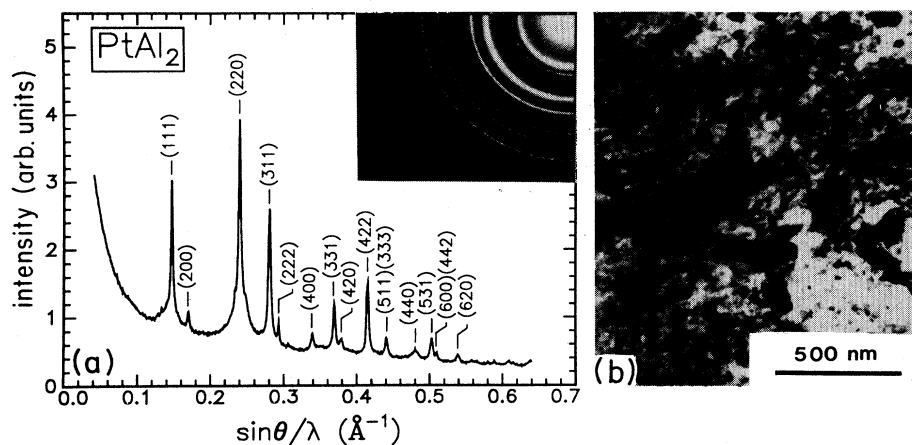

FIG. 3. (a) Selected-area-diffraction pattern of sample B in the crystallized state (selected-area aperture diameter 9.2 μm). The phase is identified as the cubic $AlPt_2$ compound. (b) Bright-field image of sample B in the crystallized state. The image shows the typical diffraction contrast of a crystalline compound.

Pt_2Al_3 for sample C.

The electrical resistivity was measured on films deposited on the oxidized Si wafers. The sheet resistance was monitored *in situ* by a four-point–probe measurement as a function of temperature in a vacuum furnace. At different stages in the annealing process, XRD was used to monitor the reaction. As the sample was heated at 0.5 °C/s, the resistivity increased to a maximum about 20 times larger than the original resistivity value, around 140 °C, which through XRD could be correlated to the disappearance of the Al and Pt crystalline peaks and the emergence of broad amorphous peaks. Around 300 °C the resistivity decreased by 12%, with the appearance of new diffraction peaks in the XRD spectrum. This confirms the description given by the TEM analysis: the initial increase in resistivity is due to the amorphization reaction and is followed by a decrease in resistivity at higher temperature as a result of crystallization.

These results let us conclude that SSA is present in the Al-Pt system and that the composition of the amorphous Al-Pt alloy is located between the compositions of the equilibrium compounds Pt_8Al_{21} and Pt_2Al_3.

IV. DISCUSSION

Adding the Al-Pt system to the list of binary SSA systems leads naturally to the question of the validity of the proposed criteria for SSA.[4] We will here address the thermodynamic (heat of mixing), kinetic (anomalous diffusion and low mobility for one of the elements in the glass phase), and structural stability (size difference) properties of the Al-Pt system pertaining to SSA.

The thermodynamic requirement proposes that SSA can only be achieved in systems with a large and negative heat of mixing. The Al-Pt system has eight intermetallic compounds,[11] a definite indication of a large negative heat of mixing.[12] This is confirmed by using the Miedema calculation.[12] For a 1:1 solid solution of Al and Pt, one obtains a value of −55 kJ/mol atom.

The proposed kinetic criteria for SSA are anomalous diffusion (e.g., as in the case of Ni in Zr) and a very low mobility of one of the elements in the amorphous phase. We have strong evidence that Al is the dominant moving species during the amorphization reaction, while the Pt mobility in the amorphous alloy is low enough to prevent nucleation at 200 °C. Namely, the low-temperature dissolution of Al in a coevaporated amorphous Al-Pt alloy[8] shows that Al diffusion in the amorphous phase is significant at these temperatures. Although the Al diffusion is fast, the mobility of Pt in the amorphous layer has to be very small; otherwise there would be no kinetic barrier for nucleation of the crystalline phase. Although Al is the fast diffuser in the amorphous alloy, it is not known to be an anomalous diffuser in Pt:[13] the Al impur-

ity diffusion and the Pt self-diffusion coefficients are within the same order of magnitude over a wide temperature range.

Finally, the Egami criterion[6] is a structural stability criterion used in the evaluation of the composition range of amorphous alloys. It describes the composition range over which the crystalline solid solution of a binary alloy becomes topologically unstable due to the atomic-size difference of the two elements A (the smaller atom) and B involved. The composition region $[x_{min}, x_{max}]$ for the amorphous alloy A_xB_{1-x} is, to first order, defined by[6]

$$x_{min} = 2\lambda \frac{R_B^3}{R_B^3 - R_A^3} , \tag{1}$$

$$x_{max} = 1 - 2\lambda \frac{R_A^3}{R_B^3 - R_A^3} , \tag{2}$$

where R_A and R_B are the atomic radii of atoms A and B, and λ is a parameter. Liou and Chien[14] applied Eqs. (1) and (2) to cosputtered glassy alloys to obtain $0.07 \leq 2\lambda \leq 0.09$. In our case, the size difference between Al and Pt is very small ($R_{Al} = 1.43$ Å and $R_{Pt} = 1.39$ Å) and a calculation using the value of λ obtained by Liou and Chien results in $x_{min} = 0.98$ and $x_{max} = 0.10$, meaning that no region of stability for the amorphous alloy is expected. Obviously, the current form of the Egami criterion is not valid for the Al-Pt system.

V. CONCLUSION

In conclusion, we have found that a solid-state amorphization reaction occurs between crystalline Al and Pt layers during low-temperature annealing. The amorphous alloy compositional region is situated between the compositions of the equilibrium Pt_8Al_{21} and Pt_2Al_3 compounds. The properties of the binary Al-Pt system are in agreement with some of the proposed criteria for systems showing SSA: it has a high and negative heat of mixing and Pt has a low mobility in the amorphous Al-Pt alloy. However, this system does not show anomalous diffusion and has only a very small difference in atomic size between the two elements, in disagreement with the current state of the Egami criterion.

[1]X. L. Yeh, K. Samwer, and W. L. Johnson, Appl. Phys. Lett. **42**, 242 (1983).

[2]R. B. Schwarz and W. L. Johnson, Phys. Rev. Lett. **51**, 415 (1983).

[3]S. R. Herd, K. N. Tu, and K. Y. Ahn, Appl. Phys. Lett. **42**, 597 (1983).

[4]W. L. Johnson, Prog. Mater. Sci. **30**, 81 (1986).

[5]P. Guilmin, P. Guyot, and G. Marshall, Phys. Lett. **109A**, 174 (1985).

[6]T. Egami and Y. Waseda, J. Non-Cryst. Solids **64**, 113 (1984).

[7]L. S. Hung, M. Nastasi, J. Guylai, and J. W. Mayer, Appl. Phys. Lett. **42**, 672 (1983).

[8]J. M. Legresy, B. Blanpain, and J. W. Mayer, J. Mater. Res. 3, 884 (1988).

[9]L. R. Doolittle, Nucl. Instrum. Methods B 9, 344 (1985).

[10]M. Van Rossum, M.-A. Nicolet, and W. L. Johnson, Phys. Rev. B 29(10), 5498 (1984).

[11]A. J. McAlister and D. J. Kahan, Bull. Alloy Phase Diagrams 7, 47 (1986).

[12]A. R. Miedema, P. F. de Châtel, and F. R. deBoer, Physica B+C 100B, 1 (1980).

[13]D. Berger and K. Schwarz, Neue Huette 23, 210 (1978); G. Rein, M. Mehrer, and F. Maier, Phys. Status Solidi A 45, 253 (1978).

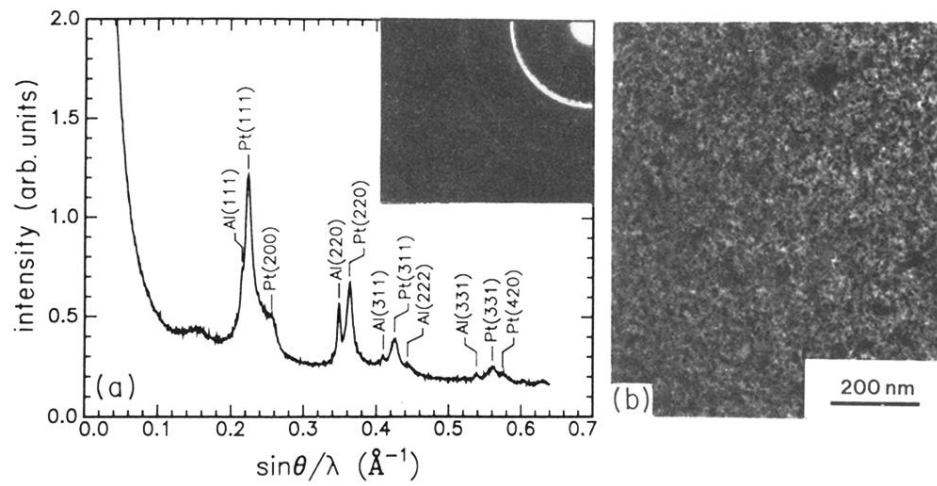[14]S. H. Liou and C. L. Chien, Phys. Rev. B 35, 2443 (1987).

FIG. 1. (a) Selected-area-diffraction pattern and microdensitometer trace of sample B in the as-deposited state. The sharp diffraction peaks can be identified as fcc Al and Pt peaks. Already we can observe the presence of broad diffraction rings of the amorphous phase (selected-area aperture diameter 3.5 μm). (b) Bright-field image of sample B in the as-deposited state. The diffraction contrast shows grains of Al ($\sim$20 nm) and Pt grains ($\sim$5 nm).
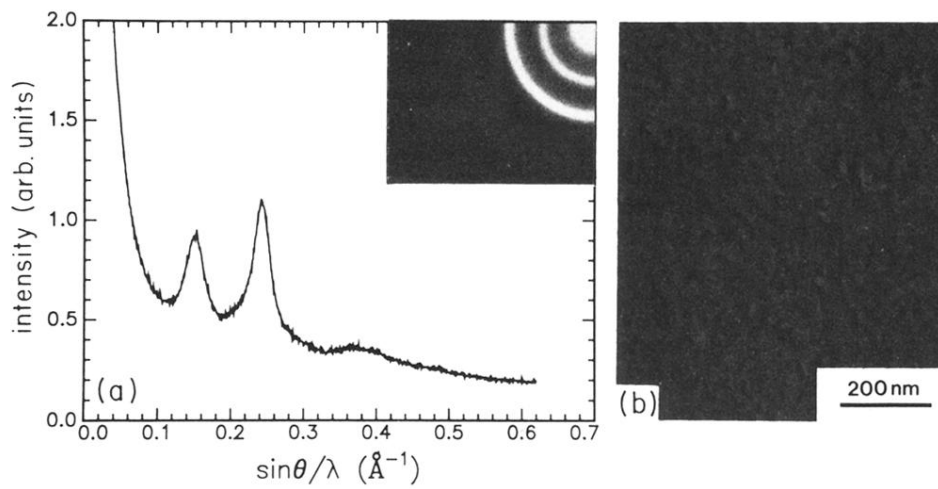
FIG. 2. (a) Selected-area-diffraction pattern of sample B in the amorphized state. Only broad rings of the amorphous alloy can be identified (selected-area aperture diameter 3.5 μm). (b) Bright-field image of sample B in the amorphized state. The contrast is main-ly flat, as is typical for an amorphous phase, although some remnants of crystallites can still be distinguished.
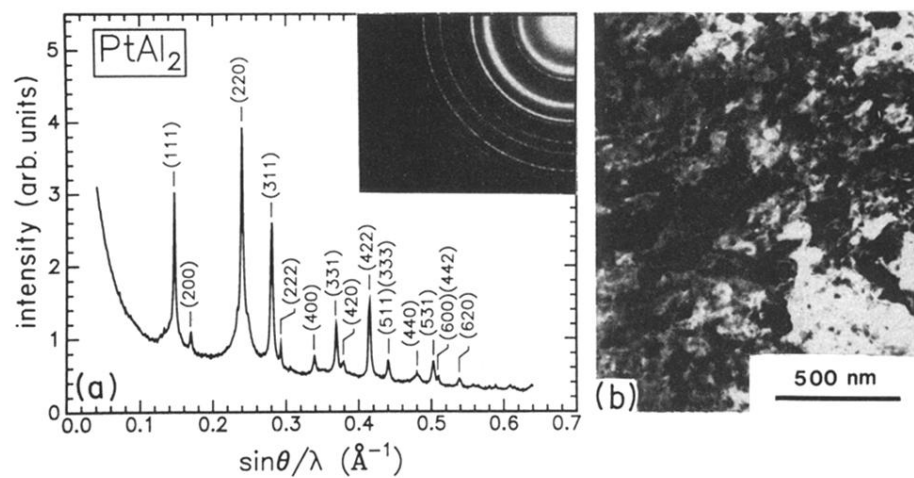
FIG. 3. (a) Selected-area-diffraction pattern of sample *B* in the crystallized state (selected-area aperture diameter 9.2 μm). The phase is identified as the cubic AlPt$_2$ compound. (b) Bright-field image of sample *B* in the crystallized state. The image shows the typical diffraction contrast of a crystalline compound.